ES Energy Environ., 2022, **18**, 65-74

ES Energy & Environment

DOI: https://dx.doi.org/10.30919/esee8c753

Cu_2NiSnS_4/Graphene Nanohybrid as a Newer Counter Electrode to Boost-up the Photoconversion Efficiency of Dye Sensitized Solar Cell

Jeniffa Rajavedhanayagam,[#] Vignesh Murugadoss,[#] Dheeraj Kumar Maurya and Subramania Angaiah[*]

Abstract

In the present work, we prepared quaternary chalcogenide (Cu_2NiSnS_4) nanoparticles and electrochemically exfoliated graphene (EEG) nanosheets to use as a nanohybrid counter electrode (CE) for Dye-sensitized solar cell (DSSC). The structural analysis revealed that the crystallite size of Cu_2NiSnS_4 in its nanohybrid is smaller than the pristine Cu_2NiSnS_4 nanoparticles. Further, it is observed from the morphological studies that the Cu_2NiSnS_4 nanoparticles are decorated uniformly over the wrinkled graphene nanosheets. The electrochemical behavior of this material is analyzed by AC impedance spectroscopy, cyclic voltammetry (CV) and Tafel polarization studies, demonstrating the synergetic effect of graphene and Cu_2NiSnS_4 in Cu_2NiSnS_4/Graphene nanohybrid. Due to the exceptional electron-transfer pathway of graphene and the excellent catalytic ability of Cu_2NiSnS_4 nanoparticles, the prepared nanohybrid exhibits excellent electrocatalytic activity towards tri-iodide reduction than the pristine Cu_2NiSnS_4 nanoparticles and graphene nanosheets. The DSSC fabricated using Cu_2NiSnS_4/graphene nanohybrid CE shows a higher photoconversion efficiency (PCE) of 7.92% than that fabricated using std. Pt (7.68%) and the prepared pristine Cu_2NiSnS_4 CE (7.20%).

Keywords: Quaternary chalcogenides; Cu_2NiSnS_4; Graphene; Nanohybrid; Counter electrode; Dye-Sensitized solar cell.
Received: 27 January 2022; Revised: 26 March 2022; Accepted: 15 July 2022.
Article type: Research article.

1. Introduction

Dye-sensitized solar cells have attracted immense research interest as an alternative to conventional solar cells because of their low cost, easy fabrication, flexibility, environmental friendliness, and high photoconversion efficiency.[1] The highest power conversion efficiency achieved till now is 14.3%. A typical dye-sensitized solar cell (DSSC) comprises dye-sensitized wide band-gap semiconductor oxide coated transparent conducting glass substrate as the photoanode, the redox couple as the electrolyte and platinum-coated transparent conducting glass substrate as the counter electrode.[2] The photoanodes are largely responsible to support dye molecules and felicitate gradual transfer of electrons to enhance conversion efficiency. Recently, ZnO, TiO_2 and SnO_2 based metal oxides with different hierarchical nanostructures (nanoparticles, nanowires & nanofibers) are reported as photoanodes for DSSCs.[3] To further improve the light harvesting capability, the anti-reflecting coating of ZnO, SiO_2, MgF_2, *etc*. on photoanode surface is adopted.[4] This strategy leads to high absorption of photons that in turn increases the free carrier density. The efficiency of DSSCs also relies on the electrolytes such as ionic liquids, polymer gel electrolytes, *etc*. These electrolytes are responsible for migration of charge carriers between electrodes and regeneration of the dye during its operation.[1] The counter electrode (CE) is the essential component in DSSC that acts as an electrocatalyst for the reduction of the triiodide (I_3^-) to iodide (I^-).[5] The main task of the CE is to collect electrons from the external circuit to regenerate the redox couple of the electrolyte at the CE/electrolyte interface. Thus, the CE materials must possess good electrocatalytic activity, large electrical conductivity, high specific surface area, low charge transfer resistance (R_{ct}), porous nature, optimal thickness, excellent adhesivity with the transparent conducting oxide (TCO), good reflectance of transmitted light, large exchange current density, good electrocatalytic ability, faster reduction of triiodide to iodide.[6]

Electro-Materials Research Laboratory, Centre for Nanoscience and Technology, Pondicherry University, Puducherry – 605014, India.

[#]These two authors contributed equally and should be treated as the first authors.

**E-mail:* a.subramania@gmail.com (Subramania Angaiah)

Generally, platinum (Pt) is used as the CE in DSSCs because of its excellent conductivity, electrocatalytic activity and lower charge transfer resistance. However, scarcity, high cost, corrosion with I^-/I_3^- redox couple inhibits the large-scale manufacturing of DSSCs.[7,8] These drawbacks accelerate the tremendous efforts to exploit the alternative CE materials in place of Pt. Various carbon materials,[9] conducting polymers,[10] metal oxides,[11] transition metal sulfides/carbides/nitrides/selenides,[12-14] quaternary chalcogenides, and their composites or nanohybrids are used as CE material for DSSCs.[15,16] Quaternary chalcogenides such as Cu_2ZnSnS_4, Cu_2FeSnS_4, and Cu_2CoSnS_4, are tremendously attracted the researchers for renewable energy applications. These materials are good for a variety of solar harvesting devices such as thin-film photovoltaics, solar water splitting, DSSCs, light emitting diodes, and battery electrodes, *etc*. because of their characteristic electronic properties with low band gap, compliance with photoelectrochemical performance, and long-term stability along with earth abundance and non-toxic nature.[17-19] Mali *et al* synthesized Kesterite Cu_2ZnSnS_4 nanofibers by electrospinning method for dye-sensitized solar cell. They used two different polymers such as polyvinylpyrrolidone (PVP) and cellulose acetate (CA) separately to prepare the Kesterite Cu_2ZnSnS_4 nanofibers. They achieved the conversion efficiency of about 3.10% and 3.90%, respectively.[20] The Cu_2NiSnS_4 resides in the group of I_2-II-IV-VI_4 quaternary chalcogenides. This is a narrow bandgap semiconductor and is significant in the field of photovoltaics.[21] It has outstanding electronic, optical and electrochemical properties.[22,23] Moreover, it is widely reported that the hybridization of the electrocatalyst with conductive carbon nanostructures such as graphene, carbon nanofibers, carbon nanotubes, *etc*. boosts their performance.[24] Also, there are no reports on quaternary chalcogenide (Cu_2NiSnS_4) decorated electrochemically exfoliated graphene-based CE for DSSC. Even though carbon black is one of the good conductive carbon materials, its resistivity is usually higher than graphene.[25] Similarly, reduced graphene oxide exhibits significantly larger electrocatalytic activity than carbon black.[26,27] In the case of mesoporous carbon, the high surface area due to its large part of micropores has a negative effect in various catalytic reactions, because the presence of micropores limits the diffusion of reactant and product and full accessibility to the supported Cu_2NiSnS_4 nanoparticles. Further, the micropores trap the Cu_2NiSnS_4 nanoparticles and make them unavailable for an electrocatalytic reaction.[28] These challenges can be overcome by using graphene. Thus, it is beneficial to develop Cu_2NiSnS_4/Graphene nanohybrid as an effective CE for DSSC. Further, various methods are available to synthesize Cu_2NiSnS_4 nanoparticles solvothermal, hydrothermal, electrospinning, hot injection process, electrodeposition, direct solution dip coating process, etc. Among them, the hydrothermal method is a simplistic approach for an abundant level of synthesis.[29]

In this work, Cu_2NiSnS_4 nanoparticles are grown *in-situ* on electrochemically exfoliated graphene nanosheets (EEG) by hydrothermal method for the first time. In our earlier works on metal chalcogenide/graphene nanohybrid as counter electrode for DSSC, the electrocatalytic activity of the counter electrode and photovoltaic performance of the fabricated devices revealed that the 1:0.50 is the optimistic mass ratio for metal chalcogenides and graphene, on comparing to the other mass ratios such as 1:0.25, 1:0.75 and 1:1.[30] Hence, the mass ratio of Cu_2NiSnS_4 to EEG is fixed as 1:0.5 for this study. The structural and morphological properties are investigated by X-ray diffraction (XRD), Raman spectroscopy, and scanning electron microscopy (SEM). The electrochemical behavior of the prepared Cu_2NiSnS_4/EEG nanohybrid as a CE for DSSC was examined. The impact of EEG nanosheets on electrocatalytic activity and photovoltaic performance is also investigated. The DSSC fabricated using Cu_2NiSnS_4/graphene nanohybrid as a counter electrode shows a higher photoconversion efficiency (PCE) of 7.92% than that fabricated using std. Pt (7.68%) and pristine Cu_2NiSnS_4 CE (7.20%).

2. Experimental

2.1 Materials

Copper (II) chloride dihydrate ($CuCl_2{\cdot}2H_2O$), Nikel (II) chloride hexahydrate ($NiCl_2{\cdot}6H_2O$), Tin (II) chloride dihydrate ($SnCl_2{\cdot}2H_2O$), L-Cysteine, polyvinylidene fluoride (PVDF, Molecular weight = 530 000), 4-tert-butyl pyridine (TBP, 96% pure), 1-Butyl-3-methylimidazolium iodide (BMImI, 99% pure) and acetonitrile (99.5% pure) were obtained from Sigma-Aldrich. The indium tin oxide (ITO) coated glass slides were obtained from Sigma Aldrich. The TiO_2 and platinum paste were purchased from Dyesol Ltd. and the dye, Ditetrabutyl ammonium cis-bis(isothiocyanato) bis(2,2'-bipyridyl-4,4'-dicarboxylato) ruthenium(II) was procured from Sigma-Aldrich. All the chemical reagents were of analytical grade and used as received.

2.2 Preparation of Cu_2NiSnS_4/Graphene nanohybrid

The Cu_2NiSnS_4/Graphene nanohybrid was prepared by a simple hydrothermal method; 0.5 g of electrochemically exfoliated graphene (EEG) nanosheets was dispersed in 50 mL of deionized water by ultrasonication.2mmol of $CuCl_2{\cdot}2H_2O$, 1 mmol of $NiCl_2{\cdot}6H_2O$, 1 mmol of $SnCl_2{\cdot}2H_2O$ and 4 mmol of L-Cysteine were added and stirred for 30 min to obtain the mass ratio of 1:0.50. This solution was transferred into a Teflon-lined stainless-steel autoclave and heated at 200 ℃ for 12 hours. The obtained sample was washed several times with distilled water and ethanol. The sample was dried under vacuum at 40 ℃ for 6 h to get Cu_2NiSnS_4/Graphene nanohybrid. The pristine Cu_2NiSnS_4 nanoparticles were synthesized under the same reaction condition without the addition of EEG nanosheets for comparison.

2.3 Fabrication of counter electrodes

The ITO glass plates were washed with deionized water, acetone, and ethanol in an ultrasonic water bath and dried in air. The slurry coating method was used to fabricate Cu_2NiSnS_4 nanoparticles, EEG nanosheets, and Cu_2NiSnS_4/EEG nanohybrid-based CEs. 95 wt.% of as prepared CE material along with 5 wt.% PVDF (binder) were mixed with the appropriate amount of N-methyl-2-pyrrolidone (NMP) and ground well in a mortar to get a homogenous CE slurry paste. The doctor blade technique was used to coat the slurry on the ITO plates at a thickness of 12 µm followed by drying in a vacuum at 80 °C for 12 h.[31] The doctor blade technique is also used to coat the platinum paste (Dyesol Ltd.) and sintered at 450 °C for 30 min at the heating rate of 5 °C/min, which is used as a reference electrode.

2.4 Physical characterization

The morphologies and nanostructures of the prepared Cu_2NiSnS_4 nanoparticles, EEG nanosheets, and Cu_2NiSnS_4/EEG nanohybrids were analyzed by using scanning electron microscopy (Hitachi, Model: 3400N). The phase and crystallinity data were acquired by using the X-ray diffraction technique (Rigaku, Ultima IV) with nickel-filtered Cu-K_α radiation in the range of 5 to 80° with an increment of 0.02°. The Raman spectra were obtained by a confocal micro-Raman spectrometer (Renishaw RM 2000) under a 20 mW Innova Ar ion laser of 785 nm.

2.5 Electrochemical characterization

The electrocatalytic activity of Cu_2NiSnS_4 nanoparticles, EEG nanosheets, and Cu_2NiSnS_4/EEG nanohybrid was studied by using such as cyclic voltammetry (CV), AC impedance and Tafel polarization by using an electrochemical workstation (Biologic: VSP) at ambient temperature. Cyclic voltammetry measurements were carried out in a three-electrode cell comprising platinum as the counter electrode, Ag/AgCl as the reference electrode, fabricated counter electrode with the active area of 0.20 cm^2 as the working electrode and acetonitrile solution containing 0.01 M LiI, 0.001 M I_2 and 0.1 M $LiClO_4$ as the electrolyte.[32] The electrochemical AC-impedance measurements were carried out using symmetrical cell in the frequency limit between 100 kHz and 1 mHz with an AC amplitude of 10 mV. The symmetrical cells were fabricated by sandwiching the redox electrolyte between the identical counter electrodes. Tafel polarization measurements were carried out at the scan rate of 50 mV s^{-1} to verify further electrocatalytic activity and interfacial charge transfer at the electrode/electrolyte interface.[30]

2.6 Fabrication of dye-sensitized solar cells (DSSCs)

The dye-sensitized TiO_2 photoanodes were fabricated by adopting the previously reported procedures.[30,33] The ITO glass plates were washed with deionized water, acetone and ethanol in an ultrasonic bath and dried in air. The fine layer of non-porous TiO_2 film was coated on the pre-cleaned ITO plates by spin coating the 5 wt.% solutions of titanium(IV) butoxide in ethanol and annealed at 450 °C for 30 min. The TiO_2 paste (Dyesol Ltd) was coated on the non-porous TiO_2 film using the doctor blade technique and then sintered at 450 °C for 30 min. The thickness of the photoanode film was 14µm and its area was 0.23 cm^2. The sintered photoanode is cooled to room temperature and soaked into a 0.12 M $TiCl_4$ solution at 70 °C for 30 min, rinsed with water and again sintered at 450 °C for 30 min. Finally, these electrodes were immersed in a solution consisting of 3×10^{-4} M dye, Di-tetrabutylammonium cis-bis(isothiocyanato) bis(2,2'-bipyridyl-4,4'-dicarboxylato) ruthenium(II) in ethanol for 24 h. These photoanodes were washed with ethanol and then dried in the air. Finally, DSSCs were assembled by placing 60 µm thick Surlyn (Solaronix SA, SX1170 hot melt) between TiO_2 photoanode and the fabricated CE. The DSSCs were then sealed by a hot pressing at 110 °C. The I^-/I_3^- redox electrolyte composed of 0.5 M LiI, 0.05 M I_2, 0.5 M TBP and 0.5 M of 1-butyl-3-methylimidazolium iodide (ionic liquid) in acetonitrile was injected between the photoanode and counter electrode of DSSC through two small holes predrilled on the CEs. The holes were camouflaged with the help of small squares of Surlyn tape. All the fabrication procedures and characterization measurements were carried out in the ambient environment without any protective atmosphere.[34]

2.7 Photovoltaic performance of DSSCs

Photovoltaic performance of as assembled DSSCs were determined by using a calibrated AM 1.5 solar simulator (Newport, Oriel instruments USA 150W, model: 67005) with the light intensity of 100 mW cm^{-2} calibrated with a standard monocrystalline silicon solar cell (Newport, Oriel Instruments, Model: 91150V) and a computer-controlled digital source meter (Keithley, Model: 2420). The measurements were done after an aging period of 24 h. The photoelectrochemical parameters such as fill factor (FF), open circuit voltage (V_{oc}), short circuit current density (J_{sc}) and incident optical power (P_{in}) and light to electricity conversion efficiency (η) were determined by using the following Equations (1) and (2);

$$\eta(\%) = \frac{V_{max}J_{max}}{P_{in}} \times 100 = \frac{V_{oc}J_{sc}FF}{P_{in}} \times 100 \quad (1)$$

$$FF = \frac{V_{max}J_{max}}{V_{oc}J_{sc}} \quad (2)$$

where J_{sc} is the short-circuit current density (mA cm^{-2}), V_{oc} is the open-circuit voltage (V), P_{in} is the incident light power (mW cm^{-2}), and J_{max} and V_{max} are the current density (mA cm^{-2}) and voltage (V) in the J-V curves, respectively, at the maximum power output.[35]

3. Results and discussion

Figure 1 shows the XRD pattern of Cu_2NiSnS_4 nanoparticles, EEG nanosheets, and Cu_2NiSnS_4/EEG nanohybrid. The characteristic diffraction peaks of Cu_2NiSnS_4 nanoparticles observed at 2θ = 28.52°, 33.21°, 47.31°, 56.33° indicate the formation of Cu_2NiSnS_4 nanoparticles with crystallographic

planes (111), (200), (220), and (311), respectively. The data is well-indexed with the cubic Cu_2NiSnS_4 with $F\bar{4}3m$ space group symmetry (JCPDS Card No. 26-0552). No prominent impurity peaks are present in the as-synthesized Cu_2NiSnS_4 which indicates the high purity of Cu_2NiSnS_4 nanoparticles. The broad diffraction peak of graphene nanosheets is observed at $2\theta = 26.50^o$ with a corresponding d spacing of 3.36 Å, which is attributed to thin graphene layers because of its high degree of exfoliation.[36] The Cu_2NiSnS_4/EEG nanohybrid has the diffraction peaks of Cu_2NiSnS_4 nanoparticles and graphene nanosheets. The mean crystallite size was calculated by using Scherrer's equation given below;

$$d = \frac{0.89\lambda}{\beta\cos\theta} \quad (3)$$

where λ is the incident X-ray wavelength, β is the Full-Width Half Maxima (FWHM) of diffraction peak, and θ is the diffraction angle. The crystallite size of Cu_2NiSnS_4 nanoparticles and Cu_2NiSnS_4/EEG nanohybrid are 27.21 nm and 13.60 nm, respectively. The crystallite size of Cu_2NiSnS_4/EEG nanohybrid is smaller than Cu_2NiSnS_4 nanoparticles which facilitate high electrocatalytic active area for the tri-iodide reduction. The impurity peaks are not present in the Cu_2NiSnS_4 nanoparticles, revealing that a hydrothermal method is a simplistic approach to obtaining pure cubic Cu_2NiSnS_4 nanoparticles.

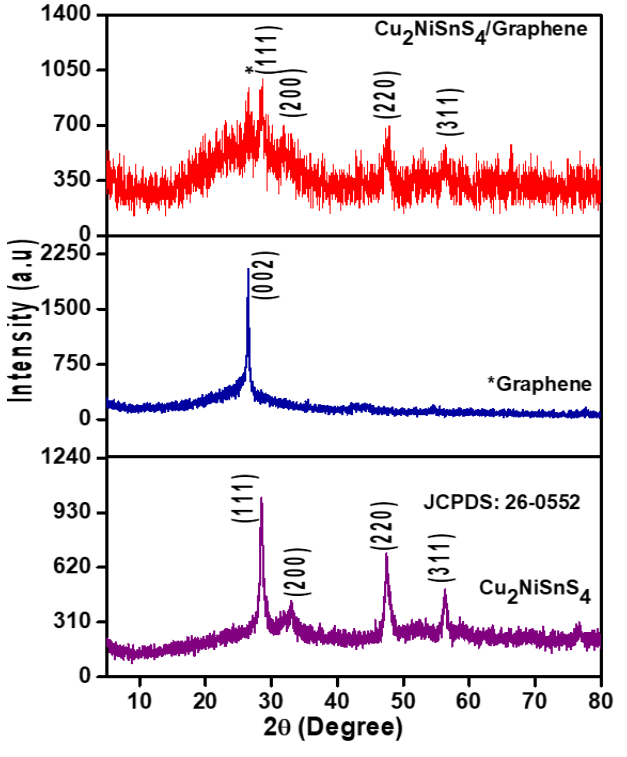

Fig. 1 XRD patterns of Cu_2NiSnS_4 nanoparticles, EEG nanosheets, and Cu_2NiSnS_4/EEG nanohybrid.

Figure 2 shows the Raman spectra of Cu_2NiSnS_4 nanoparticles, EEG nanosheets, and Cu_2NiSnS_4/EEG nanohybrid. For the Cu_2NiSnS_4 nanoparticles, the three peaks are observed at 290.15, 319.45 and 338.43 cm^{-1} indicating that the impurity phase is absent in the as-synthesized Cu_2NiSnS_4 nanoparticles. The Raman peaks are well indexed with the other quaternary chalcogenides of A_1 symmetry mode.[24] These peaks are produced by the A_1 vibrational mode of sulfur atoms surrounded by four metals (Cu, Ni, Sn, S). The characteristics and observed peak values of Raman spectra of Cu_2NiSnS_4 are given in Table 1. For graphene nanosheets, the most common D and G bands are observed at 1315 and 1600 cm^{-1}.[37] For the Cu_2NiSnS_4/EEG nanohybrid, D and G bands of graphene nanosheets together with the peaks of 292 and 334 cm^{-1} of Cu_2NiSnS_4 nanoparticles are observed. There is no impurity phase in the Cu_2NiSnS_4/EEG nanohybrid is observed, which indicates the formation of a highly pure Cu_2NiSnS_4/EEG nanohybrid.

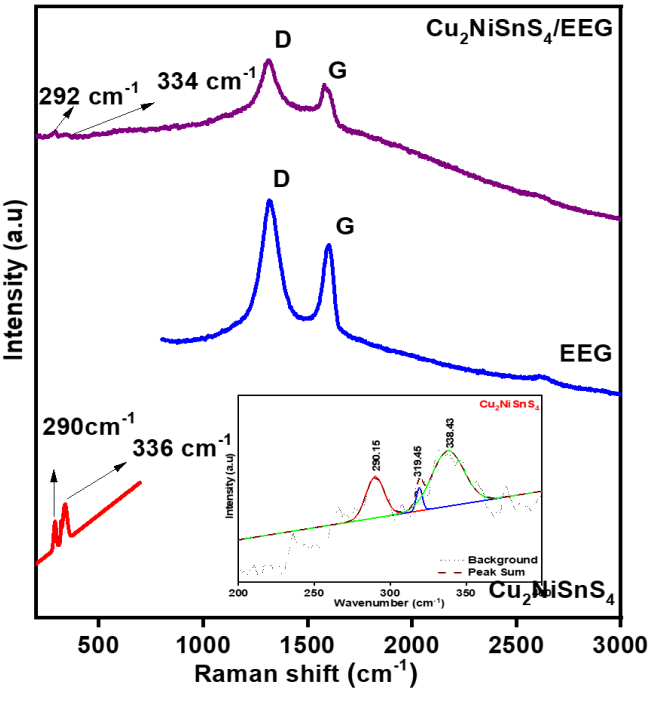

Fig. 2 Raman spectra of Cu_2NiSnS_4 nanoparticles (Inset: Deconvoluted peaks of Cu_2NiSnS_4), EEG nanosheets, and Cu_2NiSnS_4/EEG nanohybrid (Inset: Enlarged vision of Cu_2NiSnS_4 nanoparticles in the region between 200 to 500 cm^{-1}).

Table 1. The characteristic and observed peaks of Raman spectra of Cu_2NiSnS_4 nanoparticles.

Wavenumber (cm^{-1}) (Observed value)	Wavenumber (cm^{-1}) (Literature value) Ref.[38]	Symmetry
290.15	287	A_1 (Cu_2NiSnS_4)
319.45	318	A_1 (Cu_2NiSnS_4)
338.43	337	A_1 (Cu_2NiSnS_4)

Figures 3a-c indicates the SEM images of Cu_2NiSnS_4 nanoparticles, EEG nanosheets, and Cu_2NiSnS_4/EEG nanohybrid. The spherical shape of Cu_2NiSnS_4 nanoparticles is observed in Fig. 3a. Fig. 3b represents the two-dimensional pristine graphene nanosheets with a wrinkle sheet-like structure. In Cu_2NiSnS_4/EEG nanohybrid, the Cu_2NiSnS_4

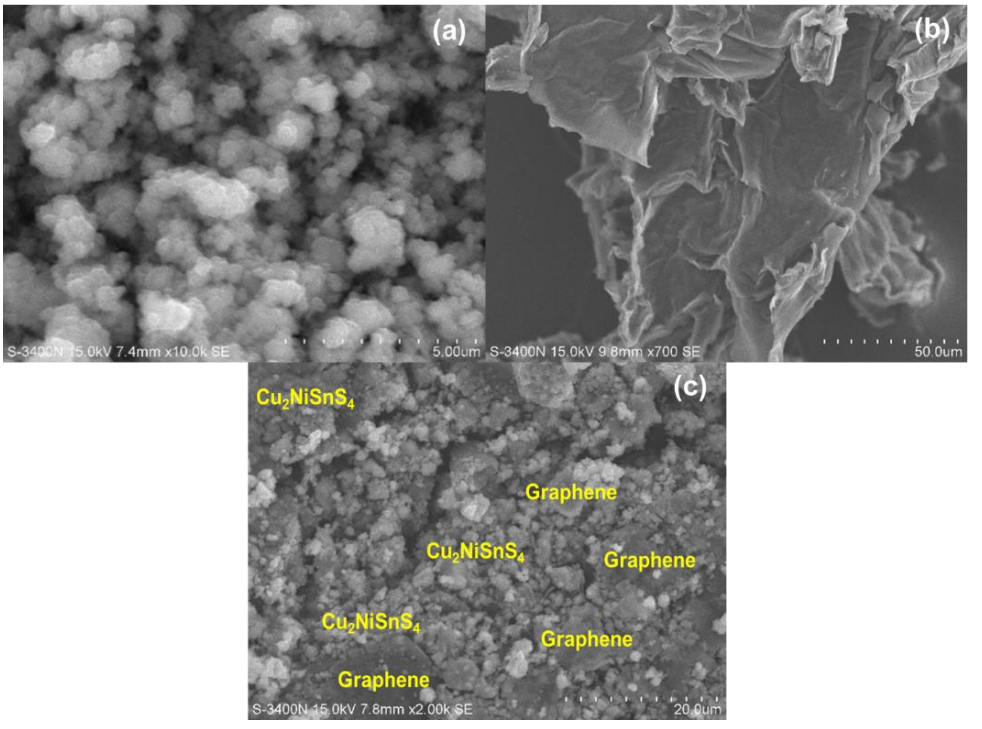

Fig. 3 SEM images of (a) Cu_2NiSnS_4 nanoparticles, (b) EEG nanosheets, and (c) Cu_2NiSnS_4/EEG nanohybrid.

nanoparticles are decorated uniformly over the wrinkled graphene nanosheets in Fig. 3c. The graphene prohibits the agglomeration of Cu_2NiSnS_4 nanoparticles and creates porous conductive network structures. The active sites are delivered by the functional groups present in the graphene nanosheets, which drives the homogeneous distribution of Cu_2NiSnS_4 nanoparticles onto graphene. The graphene contains a high surface area and supplies an improved surface-to-volume ratio to enlarge the contact area.

Figue 4 shows the Nyquist plots of symmetrical cells fabricated with Cu_2NiSnS_4 nanoparticles, EEG nanosheets, and Cu_2NiSnS_4/EEG nanohybrid. The inset represents the equivalent circuit; where, R_s is the series resistance symbolizing the resistance of the substrate, R_{ct} is the charge transfer resistance at the electrode-electrolyte interface, C_2 is its corresponding capacitance, W_2 is the Nernst diffusion impedance at the lower frequency region.[39] The equivalent circuit is employed to examine the impedance spectra fitted by using EC lab software. The measured values of $R_s$and R_{ct} are given in Table 2. Cu_2NiSnS_4/EEG nanohybrid based CE allows excellent electrocatalytic activity for I_3^- reduction in comparison with other CEs. The addition of highly electrically conductive EEG nanosheets with Cu_2NiSnS_4 nanoparticles improves the shuttling of electrons from the external circuit to the high electrocatalytic Cu_2NiSnS_4 nanoparticles, which in turn increases the reaction kinetics of tri-iodide reduction. The lower R_s value of Cu_2NiSnS_4/EEG nanohybrid indicates its excellent electrocatalytic performance that emerges from adequate electrons transport from the external circuit to the Cu_2NiSnS_4 through the two-dimensional conductive graphene. The loss of charge transportation is reduced at the interface, which improves the charge collection efficiency. This inturn

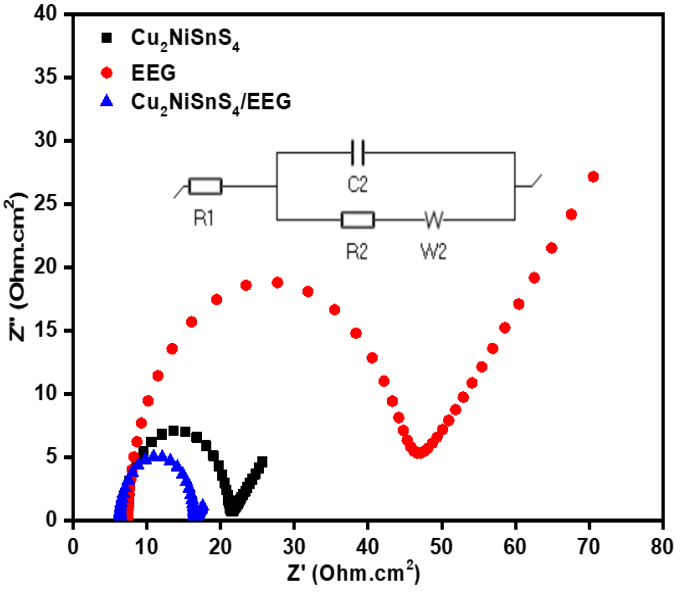

Fig. 4 Nyquist plots of Cu_2NiSnS_4 nanoparticles, EEG nanosheets and Cu_2NiSnS_4/EEG nanohybrid obtained using symmetrical cells. (Inset: Equivalent circuit).

Table 2. Nyquist, cyclic voltammetry and Tafel polarization parameters of Cu_2NiSnS_4 nanoparticles, EEG nanosheets, and Cu_2NiSnS_4/EEG nanohybrid.

Counter Electrode	R_s (Ω.cm^2)	R_{ct} (Ω.cm^2)	D_n (cm^2 s^{-1})	J_o (mA cm^{-2})
Cu_2NiSnS_4	6.92	14.59	1.19×10^{-6}	0.879
EEG	7.34	39.75	1.51×10^{-6}	0.324
Cu_2NiSnS_4/EEG	6.31	10.15	1.97×10^{-6}	1.260

will increase the photocurrent and fill factor of the DSSC fabricated using Cu_2NiSnS_4/EEG nanohybrid as the CE.

Cyclic voltammetry analysis is an effective tool to investigate the electrocatalytic activity of the prepared counter electrode by the relation between ion (I^-/I_3^-) diffusivity and reaction kinetics using three-electrode systems. The higher electrocatalytic activity towards the I^-/I_3^- the redox process is an essential factor for efficient CEs. The cyclic voltammograms show oxidation and reduction kinetics of I_3^-/I^- redox couple as follows[40];

$$3I^- \rightleftharpoons I_3^- + 2e^- \quad (4)$$

$$I_3^- + 2e^- \rightleftharpoons 3I^- \quad (5)$$

The left pair (Oxd_2/Red_2) corresponds to the redox of I_3^-/I^- and the other pair at the right (Oxd_1/Red_1) is ascribed to the redox of I_2^-/I_3^-. The cathodic peak current density (J_{pc}) of the left pair (Oxd_2/Red_2) governs the electrocatalytic activity of a counter electrode towards the triiodide reduction. The cyclic voltammograms of Cu_2NiSnS_4 nanoparticles, EEG nanosheets, and Cu_2NiSnS_4/EEG nanohybrid counter electrodes at the scan rate of 25 mV s^{-1} are shown in Fig. 5a. The cathodic peak current density (J_{pc}) values of triiodide reduction are in the order of Cu_2NiSnS_4/EEG nanohybrid (-0.338 mA cm^{-2}) > EEG nanosheets (-0.296 mA cm^{-2}) > Cu_2NiSnS_4 nanoparticles (0.263 mA cm^{-2}). The EEG nanosheets have an enormously active area, yielding a tremendous cathodic current density of Cu_2NiSnS_4/EEG nanohybrid. The larger enclosed redox reaction area of the CV curve for Cu_2NiSnS_4/EEG nanohybrid indicates a larger electrochemical active surface area. This suggests an improved electrocatalytic redox behavior of Cu_2NiSnS_4/EEG nanohybrid towards the reduction of I_3^- and oxidation of I^-. Thus, Cu_2NiSnS_4/EEG nanohybrid exhibit higher electron transfer kinetics and electrocatalytic activity than the pristine Cu_2NiSnS_4 nanoparticles and pristine EEG nanosheets. It reveals that the addition of graphene has enhanced the electrocatalytic activity of Cu_2NiSnS_4 nanoparticles towards triiodide reduction.

The CV curves at different scan rates are given in Fig. 5b. Fig. 5c indicates that the oxidation and reduction peak current densities vary linearly with the square root of the scan rate. The cathodic peak correlates to the negative direction and the analogous anodic peak correlates to the positive direction because of the increase in scan rate which represents that the interface between the counter electrode and the electrolyte is a diffusion limitation process. The diffusion coefficient (D_n, cm^2 s^{-1}) of I_3^- is measured with the cathodic peak current density of the cyclic voltammogram curves by the following Randles–Sevcik equation[41];

$$J_{pc} = K.n^{3/2}.A.C.D_n^{1/2}.\nu^{1/2} \quad (6)$$

where, J_{pc} is the peak current density of Red_2 (mA cm^{-2}), K represents the constant of 2.69 × 10^5, n indicates the number of electrons transferred in the redox process, A is the electrode area (cm^2), C is the bulk concentration of I_3^- species (mol L^{-1}),

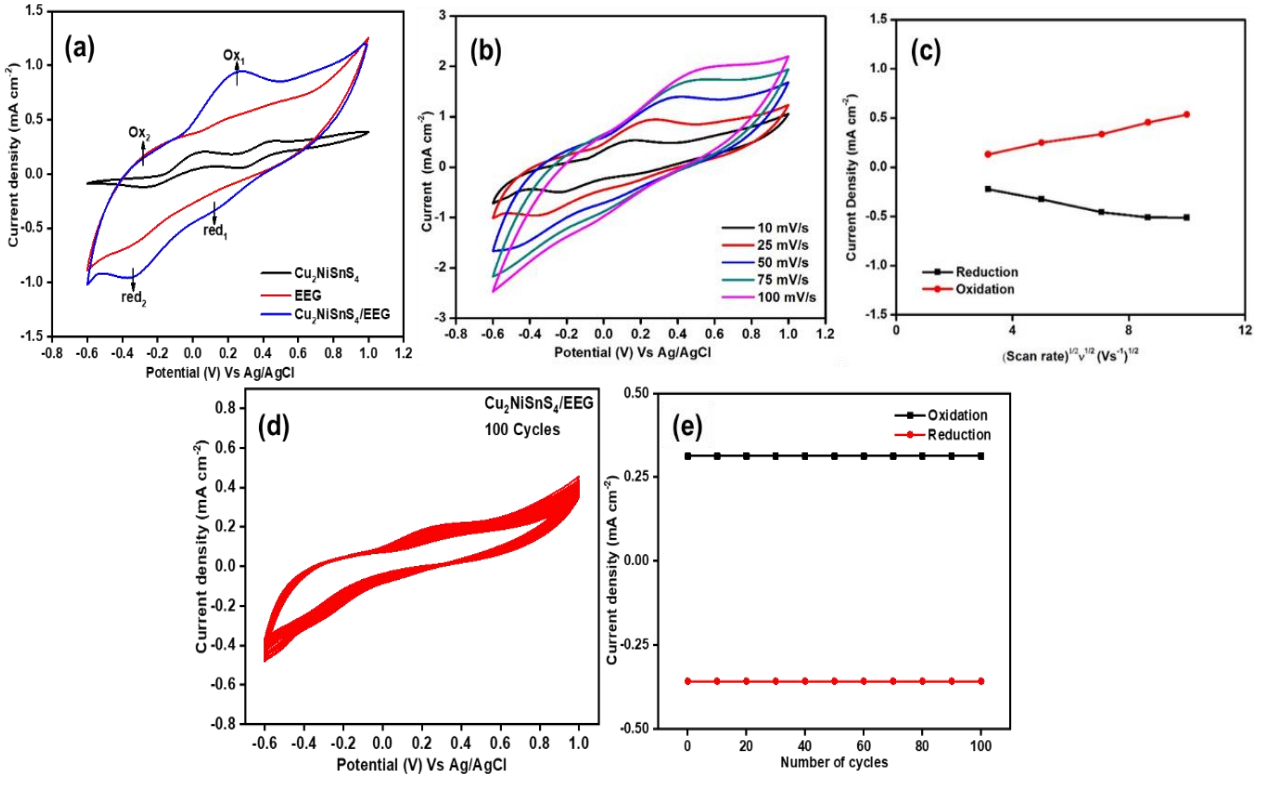

Fig. 5 (a) Cyclic voltammograms of Cu_2NiSnS_4 nanoparticles, EEG nanosheets, and Cu_2NiSnS_4/EEG nanohybrid at a scan rate of 25 mV s^{-1}; (b) The reduction and oxidation current densities of Cu_2NiSnS_4/EEG nanohybrid electrode versus square root of different scan rates; (c) Cyclic voltammograms of as Cu_2NiSnS_4/EEG nanohybrid at different scan rates; (d) Cyclic voltammograms of as Cu_2NiSnS_4/EEG nanohybrid up to 100 cycles at a scan rate 25 mV s^{-1}; (e) The relationship between the number of cycles and the maximum reduction peak current density for Cu_2NiSnS_4/EEG nanohybrid.

and ν represents the scan rate (V s^{-1}). The D_n values of I_3^- for Cu_2NiSnS_4 nanoparticles, EEG nanosheets, and Cu_2NiSnS_4/EEG nanohybrid are summarized in Table 1. The D_n values follow the trend of Cu_2NiSnS_4/EEG nanohybrid (1.97×10^{-6} cm^2 S^{-1}) > EEG nanosheets (1.51×10^{-6} cm^2 S^{-1}) > Cu_2NiSnS_4 nanoparticles (1.19×10^{-6} cm^2 S^{-1}). The greater electrocatalytic active area of Cu_2NiSnS_4/EEG nanohybrid leads to the larger value of D_n (1.97×10^{-6} cm^2 S^{-1}). Cu_2NiSnS_4 nanoparticles attached with the EEG nanosheets behave as a spacer that inhibits restacking of graphene nanosheets. Therefore, it provides a larger electrocatalytic active area and an effective diffusion pathway to the electrolyte. Fig. 5c represents the Cu_2NiSnS_4/EEG nanohybrid shows the highest stability after 100 cycles. The cathodic and anodic peak current densities (Fig. 5d) do not decrease significantly for Cu_2NiSnS_4/EEG nanohybrid CE even after 100 cycles, which indicates that Cu_2NiSnS_4/EEG nanohybrid CE is an excellent electrocatalyst for the triiodide reduction (I_3^-) with good electrochemical stability.

The interfacial charge transfer property of iodide/triiodide redox couple on the counter electrode is evaluated by Tafel plots. The logarithmic current density (J) as a function of voltage (V) at room temperature is shown in Fig. 6. The exchange current density (J_o) and the limiting diffusion current density (J_{lim}) are essential parameters to elucidate the electrocatalytic activity of the counter electrode that can be obtained from the Tafel and diffusion zone, respectively. The J_o can be determined from the intersection of the extrapolated intercepts at the linear region of the anodic and cathodic curves when zero overpotential. The Cu_2NiSnS_4/EEG nanohybrid exhibits a larger value of J_o and J_{lim} than that of pristine Cu_2NiSnS_4 nanoparticles and pristine EEG nanosheets. This confirms the higher electrocatalytic activity Cu_2NiSnS_4/EEG nanohybrid.

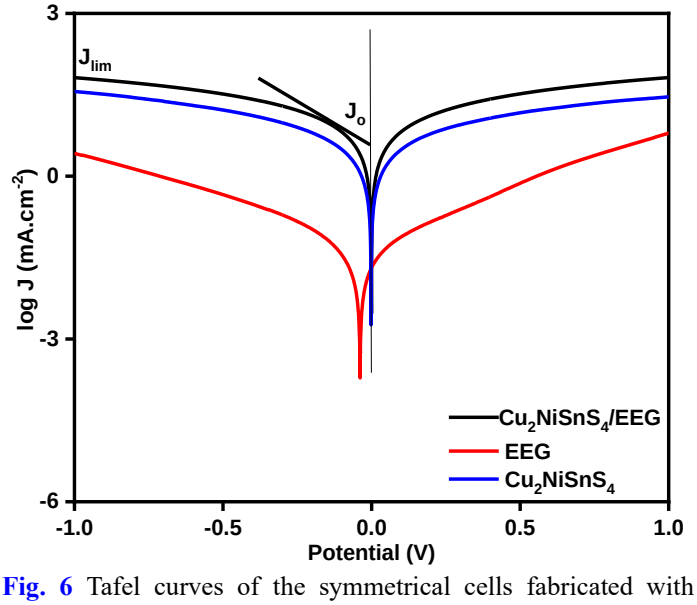

Fig. 6 Tafel curves of the symmetrical cells fabricated with Cu_2NiSnS_4 nanoparticles, EEG nanosheets, and Cu_2NiSnS_4/EEG nanohybrid.

The charge transfer resistance may be correlated with the exchange current density (J_0), while the triiodide is reduced to iodide at the counter electrode. The current exchange density is calculated from the charge transfer resistance using equation (7)[42];

$$J_o = RT/nFR_{ct} \quad (7)$$

where R, T, n, F and R_{ct} represent the gas constant, temperature, number of electrons transferred in the reduction reaction, and the Faraday constant and charge transfer resistance. Here, the value of n is two since two electrons are involved in the electrochemical reduction reaction. The exchange current density was calculated from the charge transfer resistance data, which shows the higher value of J_o for Cu_2NiSnS_4/EEG nanohybrid.

Figure 7 represents the photocurrent density-voltage (J-V) curves of the DSSCs with std. Pt, pristine Cu_2NiSnS_4 nanoparticles, and Cu_2NiSnS_4/EEG nanohybrid as the CEs, achieved at a light intensity of 100 mW cm^{-2} with the standard global AM 1.5 irradiation. The photovoltaic parameters such as short circuit current density (J_{sc}), Open circuit voltage (V_{OC}), fill factor (FF) are given in Table 3. The photovoltaic performance of Cu_2NiSnS_4/EEG nanohybrid CE is more excellent than that of std. Pt and Cu_2NiSnS_4 nanoparticles-based CEs. The DSSC assembled with Cu_2NiSnS_4/EEG nanohybrid as the CE has greater efficiency (7.92%) than that assembled with std. Pt (7.68%) and Cu_2NiSnS_4 nanoparticles (7.20%) as the CEs.

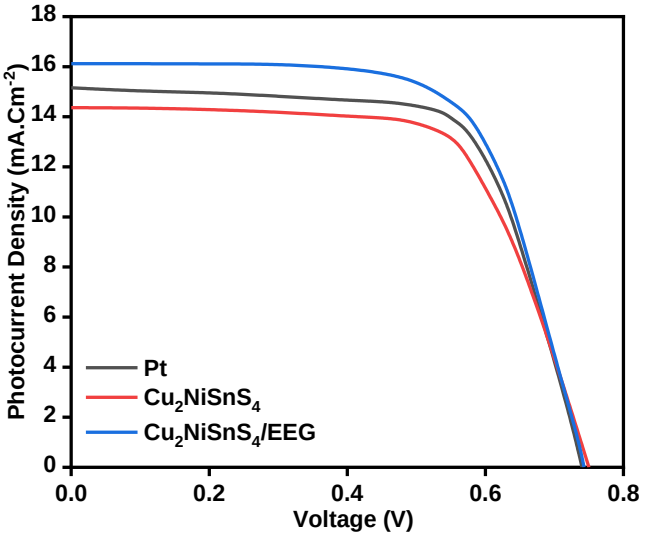

Fig. 7 J-V characteristics of DSSC fabricated with std. Pt, Cu_2NiSnS_4 nanoparticles and Cu_2NiSnS_4/EEG nanohybrid as a counter electrode.

Table 3. Photovoltaic parameters of DSSCs fabricated with std. Pt, pristine Cu_2NiSnS_4 and Cu_2NiSnS_4/EEG nanohybrid based counter electrodes.

Counter electrode	J_{sc} ($mA.cm^{-2}$)	V_{oc} (V)	FF	Efficiency (%)
Std. Pt	15.18	0.741	0.684	7.68
Cu_2NiSnS_4	14.36	0.750	0.67	7.20
Cu_2NiSnS_4/EEG	16.12	0.743	0.662	7.92

Table 4. Comparison of the photovoltaic performances of DSSCs based on Cu_2NiSnS_4/EEG with pristine Cu_2NiSnS_4 and the other reported pristine quaternary sulphides based DSSCs.

Counter Electrodes	V_{oc} (V)	J_{sc} (mA cm^{-2})	FF	Cell Efficiency η (%)	Ref.
Cu_2ZnSnS_4	0.720	12.45	0.630	5.65	[43]
Cu_2CdSnS_4	0.695	16.38	0.560	7.12	[44]
Cu_2FeSnS_4	0.705	17.37	0.570	7.36	[44]
Cu_2NiSnS_4	0.750	14.36	0.670	7.20	This work
Cu_2NiSnS_4/EEG	0.743	16.12	0.662	7.92	This work

The enhancement of (J_{sc}) in Cu_2NiSnS_4/EEG nanohybrid CE is because of the high conductive graphene, which serves as a conductive pathway for electron transfer. The EEG delivers a shortcut for the electrons to enter from the external circuit to the Cu_2NiSnS_4 nanoparticles and enhances the overall current of the redox couples (I^-/I_3^-) in the redox reaction. The comparision of the photovoltaic performance of pristine $Cu_2NiSnS_4$and Cu_2NiSnS_4/EEG nanohybrid based DSSC with other reported quaternary sulphides based DSSCs (Table 4). The Cu_2NiSnS_4/EEG nanohybrid exhibits higher photoconversion efficiency than the prepared pristine Cu_2NiSnS_4 and other reported pristine quaternary sulphides. The Cu_2NiSnS_4/EEG nanohybrid exhibits higher photoconversion efficiency than the pristine Cu_2NiSnS_4 and other reported pristine quaternary sulphides.

4. Conclusion

Cu_2NiSnS_4 nanoparticles were prepared successfully and hybrid with electrochemically exfoliated graphene nanosheets to get Cu_2NiSnS_4/EEG nanohybrid by a simple hydrothermal method. The electrochemical studies revealed that the addition of Cu_2NiSnS_4 nanoparticles onto EEG nanosheets enhances the electrocatalytic activity and faster the electron transfer kinetics for I_3^- reduction. Cu_2NiSnS_4/EEG nanohybrid exhibited a lower charge transfer resistance (10.15 Ω) than that of pristine Cu_2NiSnS_4 nanoparticles (14.59 Ω), and pristine (39.75 Ω). The Tafel plot of Cu_2NiSnS_4/EEG nanohybrid exhibited a larger value of J_o (1.260 mA cm^{-2}) and J_{lim}, further confirming its higher electrocatalytic activity, compared to pristine Cu_2NiSnS_4 nanoparticles and pristine EEG nanosheets. DSSC fabricated with Cu_2NiSnS_4/EEG nanohybrid as a CE exhibited the PCE of 7.92%, higher than that fabricated with the pristine Cu_2NiSnS_4 (7.20%) and std. Pt (7.92%) as CEs.

Conflict of Interest

There is no conflict of interest.

Supporting Information

Not applicable.

References

[1] S. Angaiah, V. Murugadoss, S. Arunachalam, P. Panneerselvam, S. Krishnan, Influence of various ionic liquids embedded electrospun polymer membrane electrolytes on the photovoltaic performance of DSSC, *Engineered Science*, 2018, **4**, 44-51, doi: 10.30919/es8d756.

[2] V. Murugadoss, S. Arunachalam, V. Elayappan, S. Angaiah, Development of electrospun PAN/CoS nanocomposite membrane electrolyte for high-performance DSSC, *Ionics*, 2018, **24**, 4071-4080, doi: 10.1007/s11581-018-2540-4.

[3] S. Angaiah, S. Arunachalam, V. Murugadoss, G. Vijayakumar, A facile polyvinylpyrrolidone assisted solvothermal synthesis of zinc oxide nanowires and nanoparticles and their influence on the photovoltaic performance of dye sensitized solar cell, *ES Energy & Environment*, 2019, **4**, 59-65, doi: 10.30919/esee8c280.

[4] P. Panneerselvam, V. Murugadoss, V. Elayappan, N. Lu, Z. Guo, S. Angaiah, Influence of anti-reflecting nature of MgF2 embedded electrospun TiO_2 nanofibers based photoanode to improve the photoconversion efficiency of DSSC, *ES Energy & Environment*, 2018, **1**, 99-105, doi: 10.30919/esee8c153.

[5] Y. Chen, Z. Jing, J. Miao, Conversion of CO_2 to 3D graphene as counter electrode for food dye-sensitized solar cells, *Journal of Electroanalytical Chemistry*, 2020, **873**, 114344, doi: 10.1016/j.jelechem.2020.114344.

[6] M. Younas, T. N. Baroud, M. A. Gondal, M. A. Dastageer, E. P. Giannelis, Highly efficient, cost-effective counter electrodes for dye-sensitized solar cells (DSSCs) augmented by highly mesoporous carbons, *Journal of Power Sources*, 2020, **468**, 228359, doi: 10.1016/j.jpowsour.2020.228359.

[7] W. C. Oh, K. Y. Cho, C. H. Jung, Y. Areerob, Hybrid of graphene based on quaternary $Cu_2ZnNiSe_4$-WO_3 nanorods for counter electrode in dye-sensitized solar cell application, *Scientific Reports*, 2020, **10**, 4738, doi: 10.1038/s41598-020-61363-x.

[8] T. Xu, W. Cao, D. Kong, X. Qin, J. Song, K. Kou, L. Chen, Q. Qiao, W. Huang, Enhanced catalytic property of transparent PEDOT counter electrodes for bifacial dye sensitized solar cells, *Materials Today Communications*, 2020, 25, 101313, doi: 10.1016/j.mtcomm.2020.101313.

[9] K. Saranya, N. Sivasankar, A. Subramania, Microwave-assisted exfoliation method to develop platinum-decorated graphene nanosheets as a low cost counter electrode for dye-sensitized solar cells, *RSC Advances*, 2014, **4**, 36226-36233, doi: 10.1039/c4ra05044d.

[10] K. Saranya, M. Rameez, A. Subramania, Developments in conducting polymer based counter electrodes for dye-sensitized solar cells - An overview, *European Polymer Journal*, 2015, **66**, 207-227, doi: 10.1016/j.eurpolymj.2015.01.049.

[11] J. Li, S. Yun, F. Han, Y. Si, A. Arshad, Y. Zhang, B. Chidambaram, N. Zafar, X. Qiao, Biomass-derived carbon boosted catalytic properties of tungsten-based nanohybrids for accelerating the triiodide reduction in dye-sensitized solar cells, *Journal of Colloid and Interface Science*, 2020, **578**, 184-194, doi: 10.1016/j.jcis.2020.04.089.
[12] K. Saranya, A. Subramania, N. Sivasankar, Influence of earth-abundant bimetallic (Fe-Ni) nanoparticle-embedded CNFs as a low-cost counter electrode material for dye-sensitized solar cells, *RSC Advances*, 2015, **5**, 43611-43619, doi: 10.1039/c5ra04963f.
[13] R. Ramachandran, S. Felix, M. Saranya, C. Santhosh, V. Velmurugan, B. P. C. Ragupathy, S. K. Jeong, A. N. Grace, Synthesis of cobalt sulfide-graphene (CoS/G) nanocomposites for supercapacitor applications, *IEEE Transactions on Nanotechnology*, 2013, **12**, 985-990, doi: 10.1109/tnano.2013.2278287.
[14] K. Saranya, A. Subramania, N. Sivasankar, S. Mallick, Electrospun TiC embedded CNFs as a low cost platinum-free counter electrode for dye-sensitized solar cell, *Materials Research Bulletin*, 2016, **75**, 83-90, doi: 10.1016/j.materresbull.2015.11.028.
[15] K. Mokurala, S. Mallick, P. Bhargava, Alternative quaternary chalcopyrite sulfides (Cu_2FeSnS_4 and Cu_2CoSnS_4) as electrocatalyst materials for counter electrodes in dye-sensitized solar cells, *Journal of Power Sources*, 2016, **305**, 134-143, doi: 10.1016/j.jpowsour.2015.11.081.
[16] S. Xu, N. Cheng, H. Yin, D. Cao, B. Mi, Electrospray preparation of $CuInS_2$ films as efficient counter electrode for dye-sensitized solar cells, *Chemical Engineering Journal*, 2020, **397**, 125463, doi: 10.1016/j.cej.2020.125463.
[17] S. Yuan, S. Wang, L. Li, Y.-H. Zhu, X.-B. Zhang, J.-M. Yan, Integrating 3D flower-like hierarchical Cu_2NiSnS_4 with reduced graphene oxide as advanced anode materials for Na-ion batteries, *ACS Applied Materials & Interfaces*, 2016, **8**, 9178-9184, doi: 10.1021/acsami.6b01725.
[18] J.-Y. Park, J. H. Noh, T. N. Mandal, S. H. Im, Y. Jun, S. I. Seok, Quaternary semiconductor Cu_2FeSnS_4 nanoparticles as an alternative to Pt catalysts, *RSC Advances*, 2013, **3**, 24918, doi: 10.1039/c3ra43331e.
[19] T.-X. Wang, Y.-G. Li, H.-R. Liu, H. Li, S.-X. Chen, Flower-like Cu_2NiSnS_4 nanoparticles synthesized by a facile solvothermal method, *Materials Letters*, 2014, **124**, 148-150, doi: 10.1016/j.matlet.2014.03.044.
[20] S. S. Mali, P. S. Patil, C. K. Hong, Low-cost electrospun highly crystalline kesterite Cu_2ZnSnS_4 nanofiber counter electrodes for efficient dye-sensitized solar cells, *ACS Applied Materials & Interfaces*, 2014, **6**, 1688-1696, doi: 10.1021/am404586n.
[21] A. Ghosh, D. K. Chaudhary, A. Biswas, R. Thangavel, G. Udayabhanu, Solution-processed Cu_2XSnS_4 (X = Fe, Co, Ni) photo-electrochemical and thin film solar cells on vertically grown ZnO nanorod arrays, *RSC Advances*, 2016, **6**, 115204-115212, doi: 10.1039/c6ra24149b.
[22] P. Pan, L. Chen, Y. Ding, J. Du, C. Feng, Z. Fu, C. Qin, F. Wang, Nitrogen-doped carbon decorated Cu_2NiSnS_4 microflowers as superior anode materials for long-life lithium-ion batteries, *Journal of Solid State Chemistry*, 2018, **261**, 103-110, doi: 10.1016/j.jssc.2018.02.021.
[23] F. Ozel, E. Aslan, B. Istanbullu, O. Akay, I. Hatay Patir, Photocatalytic hydrogen evolution based on Cu_2ZnSnS_4, Cu_2NiSnS_4 and Cu_2CoSnS_4 nanocrystals, *Applied Catalysis B: Environmental*, 2016, **198**, 67-73, doi: 10.1016/j.apcatb.2016.05.053.
[24] S. Sarkar, P. Howli, B. Das, N. S. Das, M. Samanta, G. C. Das, K. K. Chattopadhyay, Novel quaternary chalcogenide/reduced graphene oxide-based asymmetric supercapacitor with high energy density, *ACS Applied Materials & Interfaces*, 2017, **9**, 22652-22664, doi: 10.1021/acsami.7b00437.
[25] D. S. Su, S. Perathoner, G. Centi, Nanocarbons for the development of advanced catalysts, *Chemical Reviews*, 2013, **113**, 5782-5816, doi: 10.1021/cr300367d.
[26] Y. Gao, D. Ma, C. Wang, J. Guan, X. Bao, Reduced graphene oxide as a catalyst for hydrogenation of nitrobenzene at room temperature, *Chem Commun*, 2011, **47**, 2432-2434, doi: 10.1039/c0cc04420b.
[27] R. Aebersold, M. Mann, Mass spectrometry-based proteomics, *Nature*, 2003, **422**, 198-207, doi: 10.1038/nature01511.
[28] P. Ferreira, Y. Shao-Horn, D. Morgan, R. Makharia, S. Kocha, H. A. Gasteiger, Instability of Pt/ C Electrocatalysts in Proton Exchange Membrane Fuel Cells, *Journal of the Electrochemical Society,* 2005, **152**, A2256-A2271, doi: 10.1149/1.2050347.
[29] G. S. D. Babu, X. S. Shajan, A. George, P. Parameswaran, S. Murugesan, R. Divakar, E. Mohandas, S. Kumaresan, G. M. Rao, Low-cost hydrothermal synthesis and characterization of pentanary $Cu_2Zn_xNi_{1-x}SnS_4$ nanoparticle inks for thin film solar cell applications, *Materials Science in Semiconductor Processing*, 2017, **63**, 127-136, doi: 10.1016/j.mssp.2017.02.015.
[30] V. Murugadoss, N. Wang, S. Tadakamalla, B. Wang, Z. Guo, S. Angaiah, in situ grown cobalt selenide/graphene nanocomposite counter electrodes for enhanced dye-sensitized solar cell performance, *Journal of Materials Chemistry A*, 2017, **5**, 14583-14594, doi: 10.1039/c7ta00941k.
[31] V. Murugadoss, P. Panneerselvam, C. Yan, Z. Guo, S. Angaiah, A simple one-step hydrothermal synthesis of cobalt nickel selenide/graphene nanohybrid as an advanced platinum free counter electrode for dye sensitized solar cell, *Electrochimica Acta*, 2019, **312**, 157-167, doi: 10.1016/j.electacta.2019.04.142.
[32] V. Murugadoss, J. Lin, H. Liu, X. Mai, T. Ding, Z. Guo, S. Angaiah, Optimizing graphene content in a NiSe/graphene nanohybrid counter electrode to enhance the photovoltaic performance of dye-sensitized solar cells, *Nanoscale*, 2019, **11**, 17579-17589, doi: 10.1039/c9nr07060e.
[33] V. Elayappan, P. Panneerselvam, S. Nemala, K. S. Nallathambi, S. Angaiah, Influence of PVP template on the formation of porous TiO_2 nanofibers by electrospinning

technique for dye-sensitized solar cell, *Applied Physics A*, 2015, **120**, 1211-1218, doi: 10.1007/s00339-015-9306-x.
[34] Z. Salam, E. Vijayakumar, A. Subramania, N. Sivasankar, S. Mallick, Graphene quantum dots decorated electrospun TiO_2 nanofibers as an effective photoanode for dye sensitized solar cells, *Solar Energy Materials and Solar Cells*, 2015, **143**, 250-259, doi: 10.1016/j.solmat.2015.07.001.
[35] N. Singh, Z. Salam, N. Sivasankar, A. Subramania, ZnSe quantum dots sensitized electrospun ZnO nanofibers as an efficient photoanode for improved performance of QDSSC, *Materials Science in Semiconductor Processing*, 2017, **64**, 16-23, doi: 10.1016/j.mssp.2017.03.005.
[36] B. Kirubasankar, V. Murugadoss, S. Angaiah, Hydrothermal assisted in situ growth of CoSe onto graphene nanosheets as a nanohybrid positive electrode for asymmetric supercapacitors, *RSC Advances*, 2017, **7**, 5853-5862, doi: 10.1039/c6ra25078e.
[37] I. Childres, L. Jauregui, W. Park, H. Caoa, Y. P. Chena, Raman Spectroscopy of Graphene and Related Materials, *New Developments in Photon and Materials Research*, 2013, **1**, 1-20.
[38] X. Fontané, V. Izquierdo-Roca, E. Saucedo, S. Schorr, V. O. Yukhymchuk, M. Y. Valakh, A. Pérez-Rodríguez, J. R. Morante, Vibrational properties of stannite and kesterite type compounds: Raman scattering analysis of $Cu_2(Fe, Zn)SnS_4$, *Journal of Alloys and Compounds*, 2012, **539**, 190-194, doi: 10.1016/j.jallcom.2012.06.042.
[39] F. Gong, H. Wang, X. Xu, G. Zhou, Z.-S. Wang, In situ growth of $Co_{0.85}Se$ and $Ni_{0.85}Se$ on conductive substrates as high-performance counter electrodes for dye-sensitized solar cells, *Journal of the American Chemical Society*, 2012, **134**, 10953-10958, doi: 10.1021/ja303034w.
[40] Y. Wang, Y. Guo, W. Chen, Q. Luo, W. Lu, P. Xu, D. Chen, X. Yin, M. He, Sulfur-doped reduced graphene oxide/MoS_2 composite with exposed active sites as efficient Pt-free counter electrode for dye-sensitized solar cell, *Applied Surface Science*, 2018, **452**, 232-238, doi: 10.1016/j.apsusc.2018.04.276.
[41] E. S. Sowbakkiyavathi, V. Murugadoss, R. Sittaramane, S. Angaiah, Development of $MoSe_2$/PANI composite nanofibers as an alternative to Pt counter electrode to boost the photoconversion efficiency of dye sensitized solar cell, *Journal of Solid State Electrochemistry*, 2020, **24**, 2289-2300, doi: 10.1007/s10008-020-04728-6.
[42] C.-K. Cheng, C.-H. Lin, H.-C. Wu, C.-C M. Ma, T.-K. Yeh, H.-Y. Chou, C.-H. Tsai, C.-K. Hsieh, The two-dimensional nanocomposite of molybdenum disulfide and nitrogen-doped graphene oxide for efficient counter electrode of dye-sensitized solar cells, *Nanoscale Research Letters*, 2016, **11**, 117, doi: 10.1186/s11671-016-1277-0.
[43] S. Chen, A. Xu, J. Tao, H. Tao, Y. Shen, L. Zhu, J. Jiang, T. Wang, L. Pan, In-situ and green method to prepare Pt-free Cu_2ZnSnS_4 (CZTS) counter electrodes for efficient and low cost dye-sensitized solar cells, *ACS Sustainable Chemistry & Engineering*, 2015, **3**, 2652-2659, doi: 10.1021/acssuschemeng.5b00585.
[44] K. Mokurala, S. Mallick, Effect of annealing atmosphere on quaternary chalcogenide-based counter electrodes in dye-sensitized solar cell performance: synthesis of Cu_2FeSnS_4 and Cu_2CdSnS_4 nanoparticles by thermal decomposition process, *RSC Advances*, 2017, **7**, 15139-15148, doi: 10.1039/c6ra28889h.

Author Information

Jeniffa Rajavedhanayagam *is obtained her B.Tech in Nanotechnology at Noorul Islam Center for Higher Education and M.Tech in Nanoscience and Technology at Pondicherry University. Currently, she is doing her Ph.D at Scott Laboratory at the Ohio State University, Columbus Campus, United States. Her research interest includes Energy conversion and Storage devices.*

Vignesh Murugadoss, *obtained his Ph.D. from the Centre for nanoscience and Technology at Pondicherry University, Puducherry. He carried out Indo-US BASE internship at Integrated Composites Laboratory, Department of Chemical and Biomolecular Engineering at University of Tennessee, Knoxville. His research interests focus on design and development of advanced functional Nano-materials for sustainable Energy and Environmental applications.*

Dheeraj Kumar Maurya *is working as a research scholar at Electro-materials Research Laboratory, Centre for Nanoscience and Technology, Pondicherry University, Puducherry, India. His research interests include the development of electrospun nano-hybrid materials for energy storage devices and humidity sensing.*

Subramania Angaiah *is working as a Professor at the Centre for Nanoscience and Technology, Pondicherry University, India. He obtained Ph.D. degree from Alagappa University & CSIR-CECRI and his postdoctoral training from the Korean Institute of Science and Technology (KIST), Seoul, South Korea. His current research interests include the development of Nanostructured materials for M-ion Batteries, Supercapacitors, IT-SOFC, DSSC, QDSSC, PSC, Gas Sensors etc. He has published more than 150 scientific publications (h-index: 47, citations: > 7000) and filed 11 patents in INDIA, US and EU. He is also the recipient of several awards and honors like Fellow of Royal Society of Chemistry (FRSC),Fellow of Indian Chemical Society, Kolkata, Fellow of the Academy of Science, Chennai, UGC Mid-Career Award, AICTE-Career Award, etc.*